



ELSEVIER

Dynamics of Atmospheres and Oceans 32 (2000) 155–183

www.elsevier.com/locate/dynatmoce

dynamics
of atmospheres
and oceans

DAMÉE-NAB: the base experiments

Eric P. Chassignet ^{a,*}, Hernan Arango ^b, David Dietrich ^c,
Tal Ezer ^d, Michael Ghil ^e, Dale B. Haidvogel ^b, C.-C. Ma ^f,
Avichal Mehra ^c, Afonso M. Paiva ^a, Ziv Sirkes ^g

^a *Division of Meteorology and Physical Oceanography, Rosenstiel School of Marine and Atmospheric Science, University of Miami, 4600 Rickenbacker Causeway, Miami, FL 33149-1098, USA*

^b *Institute of Marine and Coastal Sciences, Rutgers University, 71 Dudley Road, New Brunswick, NJ 08901, USA*

^c *Center for Air Sea Technology, Mississippi State University, Stennis Space Center, MS 39529, USA*

^d *Program in Atmospheric and Oceanic Sciences, Princeton University, Princeton, NJ 08544-0710, USA*

^e *Department of Atmospheric Sciences and Institute of Geophysics and Planetary Physics, University of California, Los Angeles, CA 90095-1565, USA*

^f *Jet Propulsion Laboratory, California Institute of Technology, Pasadena, CA 91109, USA*

^g *The University of Southern Mississippi, Center for Ocean and Atmospheric Modeling, Stennis Space Center, MS 39529, USA*

Received 14 January 2000; received in revised form 16 February 2000; accepted 10 March 2000

Abstract

The results of an intercomparison experiment performed with five numerical ocean models of different architecture are presented. While all models are able to simulate the large-scale characteristics of the North Atlantic circulation with a fair degree of realism, they also exhibit differences that can be attributed to the choices made in vertical coordinates, domain size, and boundary conditions. © 2000 Elsevier Science B.V. All rights reserved.

Keywords: DAMÉE-NAB; Base experiments; North Atlantic circulation

1. Introduction

The overall goal of the Data Assimilation and Model Evaluation Experiment-North Atlantic Basin (DAMÉE-NAB) is to contribute to the development of an ocean

* Corresponding author. Tel.: +1-305-361-4041; fax: +1-305-361-4696.

E-mail address: echassignet@rsmas.miami.edu (E.P. Chassignet).

nowcasting capability with basin-wide forecasting skill that can provide description of the three-dimensional ocean structure, the locations of mesoscale features such as eddies and ocean fronts, and environmental definition with accuracy superior to climatology and persistence. A specific sub-goal is an evaluation of the present basin-scale numerical simulation skill in providing the large-scale information needed as boundary conditions for regional models.

Before the Navier–Stokes differential equations can be solved numerically, they must be converted into an algebraic system, a conversion process that entails numerous approximations. Numerical models have improved over the years not only because of a better physical understanding, but also because modern computers permit a more faithful representation of the differential equations by their algebraic analogs. Specifically, the discretization or “truncation” error introduced when approximating differentials by finite differences or Galerkin methods decreases as advances in computing speed and memory allow smaller and smaller mesh sizes. Rather than relying solely upon the development of computers that ultimately will allow the solutions of algebraic and differential equations to converge, numerical modelers try to reduce the truncation error in their models by using sophisticated (“higher-order”) approximations or by distributing a fixed number of grid points in physical space such that they optimally define the spatial structure of the modeled system.

It is not possible to present here an inclusive list of all existing numerical models, but they can be usually characterized by

- (a) the choice of vertical coordinate: depth, $\sigma = z/H$ (where H is the bathymetry), or isopycnic (constant density surfaces), and
- (b) the solved equations (primitive, balanced or quasi-geostrophic, hydrostatic or non-hydrostatic).

The success of any numerical simulation often depends directly on the overall model architecture. This dependence led to several comparison exercises between the various models such as DYNAMO in Europe (DYNAMO, 1997; Willebrand et al., 2000) and DAMÉE in the US (Willems et al., 1994; this issue). This overview paper reports on a series of experiments performed with five numerical models of various architectures, encompassing the wide range of choices presently available to the oceanographic community. The basic model configuration was chosen to allow a fair comparison among the models by minimizing model-specific boundary conditions. The domain size and resolution were chosen to allow additional experiments to be performed at reasonable cost by providing a benchmark, in order to explore alternative choices of boundary conditions, domain size, and horizontal and vertical resolutions. These additional experiments are the subject of the articles presented in this special issue.

The paper is organized as follows: the basic model configuration is presented in Section 2. In Section 3, the basic characteristics of the five models are presented. Section 4 discusses the various model results in comparison to available observations and previous numerical simulations. Specifically, attempts are made to identify the strengths and weaknesses common to different model classes, i.e., geopotential, sigma, and isopycnic coordinates. The results are summarized and discussed in Section 5.

2. Common configuration of the models

The computational domain (Fig. 1) is the subtropical Atlantic Ocean basin from 6°N to 50°N, including the Caribbean Sea and the Gulf of Mexico, but excluding the Mediterranean Sea. The bottom topography is derived from a digital terrain data set with 2.5' latitude–longitude resolution prepared by Z. Sirkes. The atmospheric forcing fields are based on monthly climatologies derived from the Comprehensive Ocean–Atmosphere Data Set (COADS) (Da Silva et al., 1994). The momentum forcing is given by the longitudinal and latitudinal components of the wind stress, and the mixed layer stirring rate by the oceanic friction velocity (u^*3). The thermal forcing is linearized (Da Silva et al., 1994) around climatological sea surface temperature (T_{clim}), in order to represent the model sea surface temperature (T_{mod}) feedback on the surface heat fluxes, as

$$Q = Q_{\text{net}} + \frac{dQ}{dT_{\text{clim}}}(T_{\text{mod}} - T_{\text{clim}}), \quad (1)$$

where Q_{net} and dQ/dT_{clim} are the time- and space-dependent net heat flux and air–sea coupling coefficient climatological fields, respectively. Fresh water fluxes (I) are specified as virtual salt fluxes based on the climatological evaporation (E) and precipitation (P) fields (independent of the model solution), as

$$I = - \frac{-S_0(E - P)}{\alpha}, \quad (2)$$

where S_0 is a reference salinity, and α is the specific volume of sea water.

Truly open boundary conditions, in which fluxes are specified at the boundaries, are not widely used in basin-wide simulations mainly due to the lack of information about these fluxes. It can also be argued that open boundary conditions reduce the number of degrees of freedom of the model solutions, which are forced to agree with a pre-interpre-

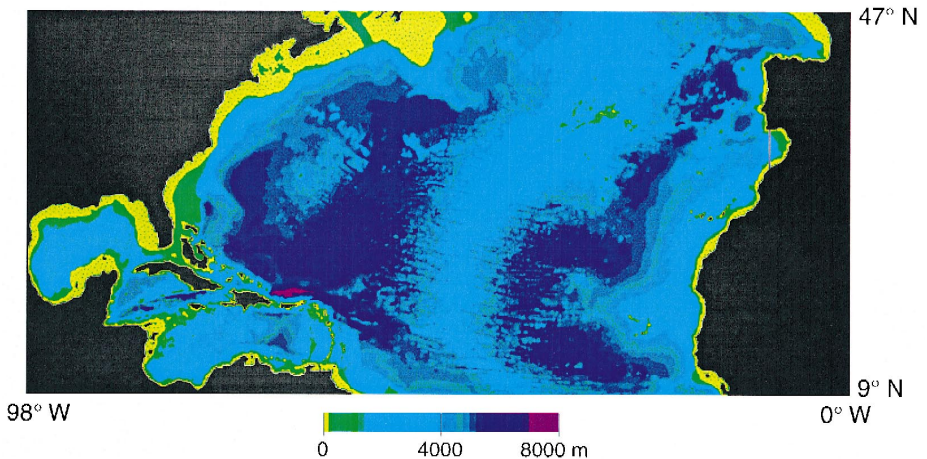


Fig. 1. Bottom topography from ETOPO 2.5 over the DAMÉE domain (buffer zones not included).

tation of the circulation at the boundaries. A more common approach for the implementation of oceanic boundary conditions, primarily because of its simplicity, has been to treat open boundaries as closed, but outfitted with buffer zones (sponge layers) in which temperature and salinity are linearly relaxed (restored) toward their seasonally varying climatological values. The main reason for use of the restoring forcing is to induce the thermohaline circulation by: (a) approximately recovering the climatological vertical shear of the currents, and (b) generating water property transformations which in reality would be accomplished in latitudes outside the model domain. The adequacy of this approach is strongly dependent upon poorly known oceanic climatologies and upon the circulation generated by the model within the buffer zones (Klinck, 1995). In particular, there is no prescription of the barotropic flow, which is free to evolve with the solution (away from the solid walls). In general, there can be no guarantee that this type of boundary condition will produce the appropriate mass, heat, and salt fluxes in the interior domain. Despite these limitations, these boundary conditions allow for a fair comparison between the models' results as one cannot "tweak" them for an optimal response. Comparisons to other approaches are performed in Ezer and Mellor (2000, this issue). The impact of placing these boundaries at 6°N and 50°N is investigated in Paiva et al. (2000, this issue) and Haidvogel et al. (2000, this issue).

The three buffer zones are located at the northern boundary and at the southern boundary (3° latitude band) and in the Gulf of Cádiz (representing the Mediterranean Sea). The restoring time scale for the boundaries varies linearly from 60 days at the inner edge to 5 days at the walls. The initial conditions are the January Levitus (1982) climatology and all models are integrated for a total of 10 years. The horizontal resolution is in the order of 0.5° (~ 50 km on average) and the vertical resolution is in the order of 20 levels/layers, depending on the model's architecture as described in more detail in Section 3.

3. Characteristics of the models

The five numerical models introduced in this section encompass the wide range of choices presently available to the oceanographic community. They all solve the hydrostatic primitive equations and are classified with respect to their vertical coordinate choices. The following sub-sections describe the salient aspects of the models, the horizontal and vertical discretization as well as the parameterization choices (lateral and vertical mixing, mixed layer). Deviations from the common configuration of Section 2 are documented if necessary.

3.1. *Depth coordinates*

3.1.1. *The Modular Ocean Model (MOM)*

The MOM is a z -coordinate ocean model developed at the Geophysical Fluid Dynamics Laboratory (GFDL) by Bryan (1969) and Cox (1984). MOM solves the three-dimensional primitive equations with the Boussinesq approximation and realistic

topography. The equations are discretized using finite differencing on a latitude–longitude Arakawa B grid in the horizontal with a rigid-lid assumption to filter out the high-frequency surface gravity waves.

The model's domain and resolution were set up according to the DAMÉE-NAB guidelines (Section 2) and were configured for the North Atlantic Basin from 6°N to 50°N and from 98°W to 10°E. Part of the Mediterranean Sea is included. A uniform $0.5^\circ \times 0.5^\circ$ horizontal resolution is used throughout the entire domain. In the vertical, the grid has 15 non-uniform levels which vary in thickness increasing with depth (the first five levels are located at depths of 2.5, 10, 24, 50, and 94 m, respectively). The model time step is 30 min. The bottom topography for the model is derived from the bathymetry dataset described in Section 2. Minor smoothing is applied to the topography before it is discretized to yield the number of “ocean” grid boxes in each vertical column. At the northern and southern boundaries of the model domain, there are two 3° -wide buffer zones in which temperature and salinity are relaxed towards the Levitus (1982) climatology; the relaxation uses an e -folding time of 5 days at the outer boundary that increases gradually to 60 days toward the inner edge of the buffer zone. The initial state of the model has climatological January mean temperature and salinity distribution and zero velocities. At the lateral boundaries, the no-slip condition is applied. For the parameterization of horizontal subgrid-scale mixing, a biharmonic mixing with constant coefficients equal to $2 \times 10^{19} \text{ cm}^4/\text{s}$ was used for both tracers and momentum. The Mellor and Yamada (1982) level 2.5 turbulence closure scheme is used for vertical mixing.

DIFFERENCES FROM THE COMMON CONFIGURATION: inclusion of a portion of the Mediterranean Sea.

3.1.2. DieCAST

The primary features of DieCAST (Dietrich, 1997) are: z -level vertical coordinates; hydrostatic; non-staggered horizontal grid (i.e., no spatial discretization errors in the formulation of the Coriolis terms); fourth-order-accurate pressure gradient and advection terms; rigid-lid approximation; direct calculation of convective adjustment. As noted by Kreiss and Ystrom (1998) and Browning et al. (1998), fourth-order accuracy greatly facilitates the representation of nonlinear cascade dynamics, especially when the Rossby radius of deformation is resolved by the grid (Dietrich, 1997; Dietrich and Ko, 1994; Dietrich and Lin, 1994; Dietrich et al., 1997). Further arguments favoring fourth-order-accurate differencing are given by Sanderson (1998) and Sanderson and Brassington (1998).

The horizontal resolution is 0.5° with the grid spacing varying with the cosine of latitude. The vertical resolution consists of 20 levels with the shallowest level being at 20 m and the remaining levels configured in a downward expanding grid. The time step is 60 min. The unfiltered raw DAMEE-NAB bathymetry is used as follows to create the bathymetry used in the model: (a) the raw depth data are interpolated to model cell centers, except in a small Florida Straits area, where the deepest point in each model 0.5° control volume area is used in order to give a more realistic choke point representation in the poorly resolved Florida Straits; (b) the conventional stairstep approximation of z -level models is applied to the interpolated depth data.

DieCAST requires very little total dissipation for numerical stability. The model dissipation parameters are the following: standard nonlinear drag coefficient (0.002), horizontal viscosity and diffusivity equal to $20 \text{ m}^2/\text{s}$, vertical viscosity and diffusivity equal to a $1 \text{ cm}^2/\text{s}$ background value multiplied by an amplification factor, plus a contribution based on vertical cell Reynolds number. The amplification factor is specified latitudinally and is depth- and season-dependent; its maximum occurs during winter in the top layer at the northernmost latitude. The factor decreases by 10% per latitude zone and 50% per layer from its maximum location. Its time dependence is a 1-year period sine wave with a maximum value of 10 during the summer and 50 during the winter. The maxima are always at the northernmost top layer point. This simple mixed layer parameterization in the turbulent cooled high latitude near surface regions allows the model's own internal convective plume dynamics to complete convective adjustment associated with deep water formation in a non-diffusive way, thus avoiding the need for convective adjustment schemes (Dietrich and Mehra, 1998).

DIFFERENCES FROM THE COMMON CONFIGURATION: none.

3.2. *Sigma coordinates*

The concept of terrain-following (or sigma) coordinates was first introduced in atmospheric modeling (Phillips, 1957) and has since become a common alternative in large-scale and regional ocean circulation modeling.

3.2.1. *The Princeton Ocean Model (POM)*

The POM is a free surface, sigma coordinate model in which the hydrostatic, primitive equations are solved on a horizontal curvilinear orthogonal coordinates and an Arakawa C finite differencing grid. The horizontal time differencing is explicit whereas the vertical differencing is implicit. The latter method eliminates time constraints for the vertical coordinate when a fine vertical resolution is used in the surface or bottom boundary layers. Since the model has a free surface, a split time step is used; a shorter time step is used for solving the vertically integrated, two-dimensional equations (the external mode) and a longer time step is used for solving the three-dimensional equations (the internal mode). The vertical coordinate is defined by $\sigma = (z - \eta)/(H + \eta)$, so that $\sigma = 0$ at the surface $z = \eta$ and $\sigma = -1$ at the bottom $z = -H$. The model has full thermodynamics. An equation of state formulated by Mellor (1991), which simplifies the full UNESCO formulation, is used. The details of the numerical code can be found in Blumberg and Mellor (1987).

For the standard DAMÉE-NAB configuration, there are 16 unevenly distributed vertical sigma layers with higher resolution in the upper mixed layer and lower resolution in the deep ocean. The horizontal grid employs a curvilinear orthogonal system with a variable resolution covering the domain from 5°N to 50°N and 0°W to 100°W . The grid resolution ranges from $\sim 20\text{--}35 \text{ km}$ in the Gulf of Mexico and the Gulf Stream to $\sim 50 \text{ km}$ in the eastern North Atlantic (see Ezer and Mellor, 2000, this issue, for more detail). The bottom topography in the model has been smoothed following Mellor et al. (1994) to minimize pressure gradient errors; the maximum ocean

depth in the model is 5500 m and the minimum depth is 10 m so that the continental slope and shelf are included.

The vertical mixing coefficients are provided by the Mellor and Yamada (1982) turbulence scheme, so that the mixed layer properties are the result of the model dynamics. However, because of inconsistencies between the surface buoyancy fluxes and the climatology used for initialization and for the lateral buffer zones, it was found necessary to add a weak relaxation of salinity to the monthly climatology in the mixed layer in order to reduce unrealistic changes in the mixed layer. The horizontal mixing coefficients for momentum and tracers are calculated by a Smagorinsky-type formulation (Smagorinsky et al., 1965); thus they are spatially dependent on velocity gradients and grid size. The turbulence Prandtl number is equal to 1 and the Smagorinsky coefficient is equal to 0.1; the resultant diffusion in the upper ocean is therefore in the range 100–2000 m²/s. See Ezer and Mellor (2000, this issue) for more details about the horizontal diffusion formulation and the model sensitivity to changes of those parameters.

The initial conditions are the January climatological temperature and salinity data of the Generalized Digital Environmental Model (GDEM) (Teague et al., 1990). Lateral boundary conditions for temperature and salinity are provided by three 3°-wide buffer zones, in the north, south, and east (west of the Gibraltar Straits, which are closed), in which model fields are relaxed towards the GDEM monthly climatology with relaxation time scale ranging from 5 days near the boundary to 60 days at the outer edge of the buffer zone.

DIFFERENCES FROM THE COMMON CONFIGURATION: relaxation to climatological salinity for the upper five sigma-levels (relaxation time ranging from 30 days at the surface to 360 days at level 5), variable grid.

3.2.2. *The Regional Ocean Modeling System (ROMS)*

The ROMS is the latest in a series of terrain-following model hierarchies that originated with the Semi-spectral Primitive Equation Model (SPEM) (Haidvogel et al., 1991) and continued with the S-coordinate Rutgers University Model (SCRUM) (Song and Haidvogel, 1994). A detailed description of these model hierarchies can be found in Haidvogel and Beckmann (1999). ROMS was completely rewritten for efficiency in single and multi-threaded computer architectures, and was expanded to include a variety of new features including high-order advection schemes; more accurate pressure gradient algorithms; and a unified set of atmospheric, oceanic, and benthic boundary layers. A valuable feature, first introduced in SCRUM, is a generalized nonlinear terrain-following coordinate that can be configured to provide enhanced resolution at either the sea surface or sea floor. See Haidvogel et al. (2000, this volume) for a discussion of the impact of this generalized coordinate.

In ROMS, the hydrostatic primitive equations are approximated using boundary fitted, orthogonal curvilinear coordinates on a staggered Arakawa C-grid. The horizontal stencil utilizes centered, second-order finite differences. In the vertical, the equations are discretized over variable topography using stretched terrain-following coordinates (Song and Haidvogel, 1994) which allow increased resolution in areas of interest — e.g., the

oceanic surface and bottom boundary layers. As in the horizontal, the default stencil uses centered, second-order finite differences on a staggered vertical grid.

As in POM, the hydrostatic primitive equations for momentum are solved using a split-explicit time-stepping scheme in which the barotropic (fast) and baroclinic (slow) modes are separately advanced in time. In ROMS, the separated time-stepping is constrained to maintain exactly both volume conservation and constancy preservation of the tracer fields. The resulting equations are time-discretized using a third-order accurate predictor (Leap-Frog) and corrector (Adams–Moulton) time-stepping algorithm which is very robust. The enhanced stability of the scheme allows larger time steps, by a factor of about four, which more than offsets the increased cost of the predictor-corrector algorithm.

In the experiment described here, ROMS has been configured with 20 terrain-following coordinate levels and the horizontal resolution is set to $3/4^\circ$. The baroclinic and barotropic time-steps are 5400 and 200 s, respectively. The advection scheme is fourth-order, centered differences for the predictor step, and third-order, upstream biased for the corrector step. The latter scheme has a velocity-dependent hyper-diffusion dissipation as the dominant truncation error (Shchepetkin and McWilliams, 1998), so there is no need for explicit horizontal viscosity or diffusion; explicit viscous and diffusive coefficients are therefore set to zero. The vertical mixing parameterization is based on the nonlocal, K-profile, boundary layer formulation of Large et al. (1994).

DIFFERENCES FROM THE COMMON CONFIGURATION: $3/4^\circ$ grid spacing.

3.3. Isopycnic coordinates

3.3.1. The Miami Isopycnic Coordinate Ocean Model (MICOM)

The most significant aspect of the MICOM architecture is the vertical discretization in layers of constant density. The fundamental reason for modeling ocean flow in density coordinates is that this system suppresses the diapycnal component of numerically caused dispersion of material and thermodynamic properties (temperature, salinity, ...). This characteristic allows isopycnic models to prevent the spurious warming of deep water masses, as has been shown to occur in models framed in Cartesian coordinates (Chassignet et al., 1996). Furthermore, the association of vertical shear with isopycnal packing and tilting in the ocean makes isopycnic models appropriate for studies of strong baroclinic currents, such as the Gulf Stream. For a review, the reader is referred to Bleck et al. (1992) and Bleck and Chassignet (1994).

In the experiment reported in this paper, the vertical density structure is defined by 15 isopycnic layers, with σ_θ values of 24.70, 25.28, 25.77, 26.18, 26.52, 26.80, 27.03, 27.22, 27.38, 27.52, 27.64, 27.74, 27.82, 27.88, and 27.92, topped by a dynamically active Kraus–Turner surface mixed layer. The vertical discretization was chosen in order to provide higher resolution in the upper ocean. The horizontal grid is defined on a Mercator projection, with the 0.5° grid interval fixed in the longitudinal direction, but varying with the cosine of latitude (Bleck et al., 1992).

Subgrid-scale mixing is parameterized as proportional to the grid size (Δx), and momentum, thickness, and temperature/salinity diffusion coefficients are expressed as $u_d \Delta x$ (Bleck et al., 1992). The diffusion velocity u_d has values of 1.0, 0.2, and 0.5

cm/s for momentum, thickness, and temperature/salinity, respectively. Mixing of momentum is enhanced in zones of strong horizontal shear, as a function of the deformation tensor (Smagorinsky, 1963) with a proportionality factor of 0.1. The diapycnal mixing coefficient is $10^{-3}/N \text{ cm}^2 \text{ s}^{-2}$ for all experiments, where N is the Brunt–Väisälä frequency.

DIFFERENCES FROM THE COMMON CONFIGURATION: none.

4. Results

All models have been integrated for at least 10 years, a short time compared to the thermohaline response of the deep ocean, but sufficient for the circulation fields to be adjusted to the density distribution. The velocity fields reached a dynamical quasi-equilibrium state after 5 years (Paiva et al., 2000; Haidvogel et al., 2000; both in this issue), and the last 3 years of the runs were used as the analysis time period.

4.1. Meridional overturning streamfunction and associated heat flux

The zonally integrated overturning transport (Fig. 2) characterizes the thermohaline circulation established in response to the external forcings (heat and freshwater fluxes) and to the water mass conversions taking place in the buffer zones. The magnitude of the circulation varies considerably among the models from a low of 12 Sv in ROMS to a high of 21 Sv in MOM. In all models, the maximum transport is between 1000 and 1500 m deep. The spatial structure of the thermohaline cells are however distinctly different, implying different pathways for the deep-water flows.

Despite the 3-year time average, the sigma-coordinate model POM exhibits several secondary thermohaline cells around 1000 m depth. These secondary closed recirculations are responsible for the oscillations of up to 0.2 PW that are observed in the meridional heat transport of POM (Fig. 3). POM, when compared to the other models, also exhibits some additional sinking around 25°N below 3000 m with water masses moving poleward. The shallow (200 m) negative cells north of 25°N, observed in all models, are also more pronounced in POM. The meridional overturning streamfunction and associated heat flux in the other sigma-coordinate model ROMS show much less variability as a function of latitude, but also a much weaker circulation and heat transport (by about 40%) (Figs. 2 and 3).

The level models, DieCAST, and MOM, exhibit the traditional spurious upwelling around 35°N associated with the Gulf Stream when integrated without the Gent and McWilliams (1990) isopycnal parameterization of eddy mixing (Böning et al., 1995). MOM also has a deep reverse cell of about 7 Sv extending to 35°N, which is traditionally attributed to the penetration of Antarctic Bottom Water (AABW) into the North Atlantic. There is no AABW in MICOM as it cannot be represented by the σ_θ discretization (Sun et al., 1999). In the sigma-coordinate simulations, the northward AABW penetration is either very small (ROMS) or non-existent (POM). A small countercirculation cell of unknown source is also present in POM north of 25°N and below 3000 m.

The 3-year mean meridional heat transport associated with the overturning circulation is presented in Fig. 3c. Except for ROMS, the magnitude of the transport is similar for

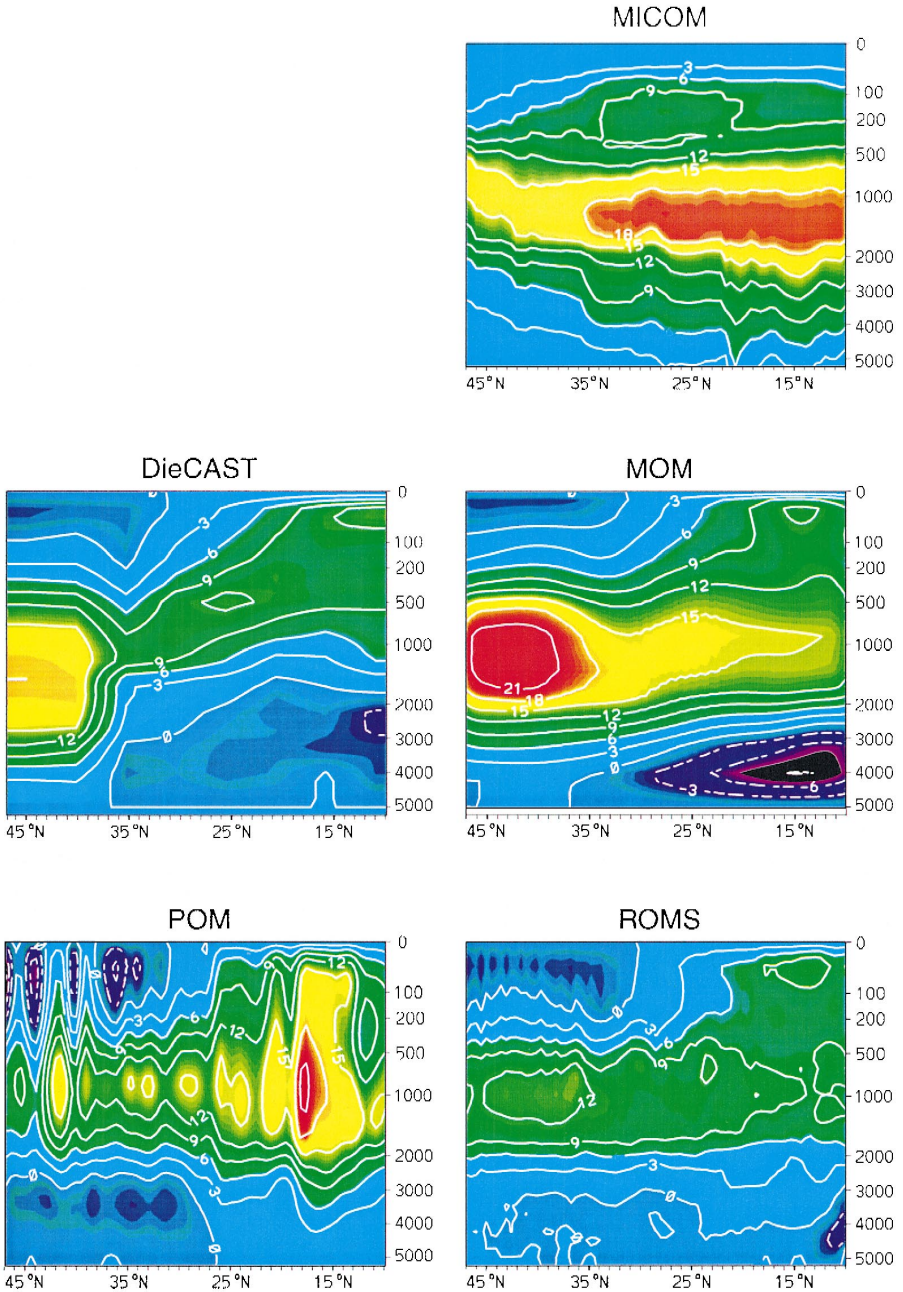


Fig. 2. Meridional overturning streamfunction for the five models. The contour interval is 3 Sv.

all models with a maximum of 1.1–1.2 PW, in agreement with observations (Macdonald and Wunsch, 1996). The latitudinal position of this maximum varies significantly among

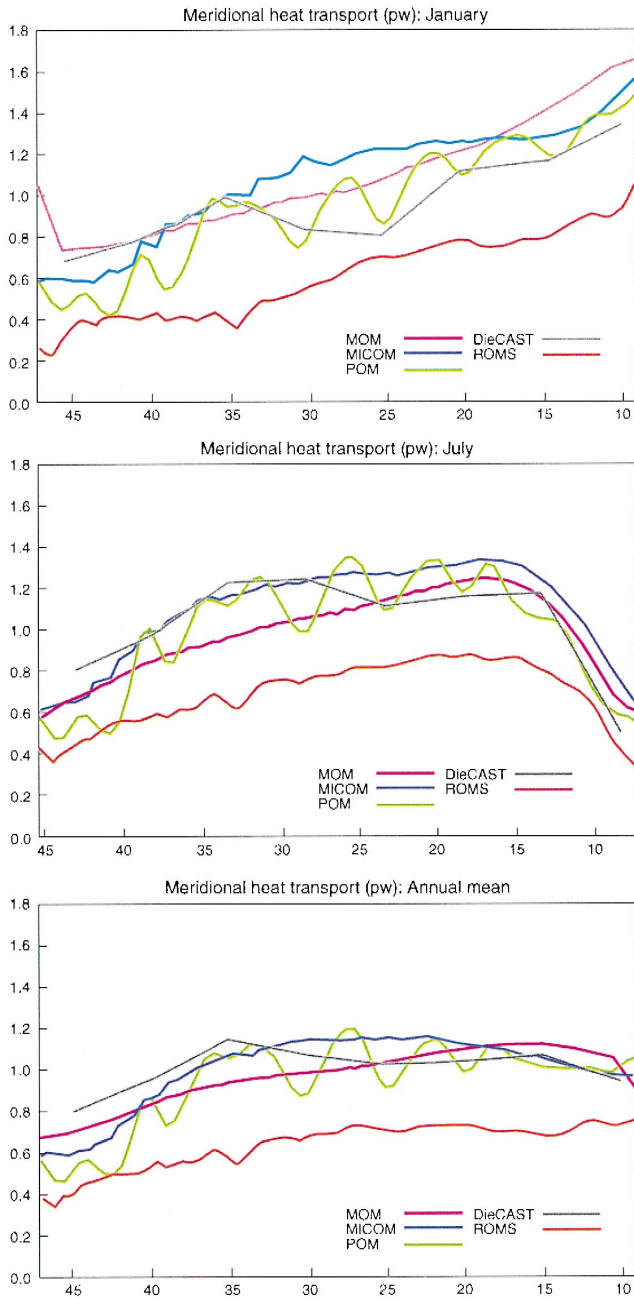


Fig. 3. Meridional heat transport for the five models in Petawatts. (a) 3-year January mean, (b) 3-year July mean, (c) 3-year annual mean.

the models, however, especially in POM which exhibits several secondary maxima. These maxima are associated with the secondary thermohaline cells present in the zonally integrated transport for this experiment (Fig. 2). The heat transports are also shown for the months of January and July (3-year time average) in Fig. 3a and b, respectively. As for the mean, the magnitude of the transport variations is similar for all models, with the exception of ROMS which is weaker. The largest temporal fluctuations (~ 1 PW) are observed in the tropics and are primarily wind-driven (Böning and Herrmann, 1994). Except for ROMS, the maximum is around 1.6 PW in summer and the minimum is around 0.5 PW in winter, in agreement with previous model estimates (Böning and Herrmann, 1994; Chassignet et al., 1996).

4.2. Surface circulation

The mean sea surface elevation (Fig. 4) provides a first-order estimate (geostrophic component) of the surface circulation. Non eddy-resolving simulations usually exhibit an

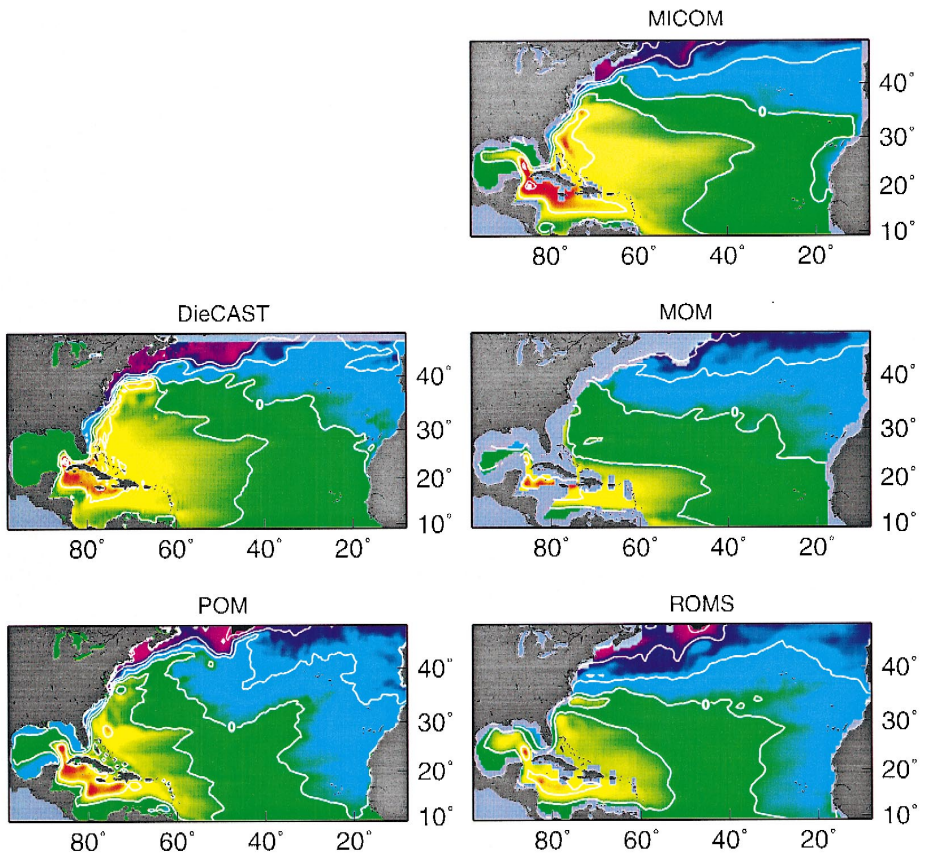


Fig. 4. Three-year time average sea surface height for the five models. For MOM, the sea surface height was derived from the 1000 m geopotential height. The contour interval is 2×10^{-1} m.

overshooting Gulf Stream. This is effectively the case for most of the model results displayed in Fig. 4 with the exception of ROMS, which displays a Gulf Stream path after separation at approximately the latitude of Cape Hatteras.

The position of the Gulf Stream North Wall (defined by the 15°C isotherm at 200 m) during the last 3 years of the ROMS integration are displayed in Fig. 5. In this simulation, the Gulf Stream overshoots, eventually separates at 40°N, and then re-enters the interior at 38°N. The path then moves gradually south. Except for the overshooting, a similar behavior for the Gulf Stream path is also observed with ROMS in a series of companion experiments performed with a larger North Atlantic domain (northern boundary at 65°N) by Haidvogel et al. (2000, this issue) (Fig. 12). Haidvogel et al. suggest that the southern separation is due to a strong southward excursion of the Labrador Current into the Mid-Atlantic Bight, resulting from an overly vigorous subpolar gyre. However, since in the smaller domain configuration, the Labrador Current is non-existent and its influence on the interior circulation is only via the buffer zones, one could therefore argue that the southern separation in ROMS may in fact result from some of the numerical choices that were made therein. This aspect requires further investigation.

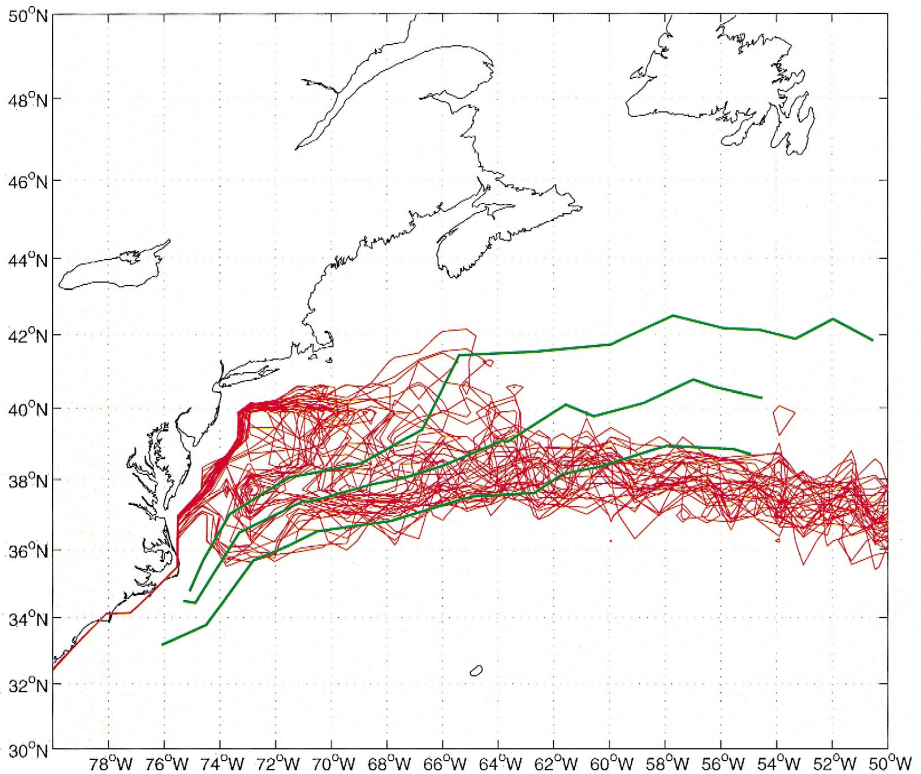


Fig. 5. ROMS monthly means of the Gulf Stream north wall for years 8–10 derived from the 15°C isotherm at 200 m. The black lines are the TOPEX 1992–1994 mean and extreme locations (Lee, 1997).

The sensitivity of the Gulf Stream separation to the strength of the southward flow at 47°N was also discussed by Ezer and Mellor (2000, this issue) in a series of sensitivity experiments performed with POM as a function of the northern boundary condition (open versus closed). While open boundary conditions with a specified inflow at the northern latitude improve somewhat the separation process, it does not appear to be a controlling factor in these experiments. Other processes, such as interaction with bottom topography and inertia (Dengg et al., 1996; Özgökmen et al., 1997), surface heat fluxes (Ezer and Mellor, 1992; Chassignet et al., 1995), or inter-annual variability of the separation point (Jiang et al., 1995), need to be taken into account.

At the 0.5° resolution used by most of the models, internally generated variability on the mesoscale is weak and most of the fluctuations are generated by the seasonal atmospheric forcing. In all experiments (Fig. 6), mesoscale variability is effectively small over most of the domain when compared to observations (Fig. 6a). Higher

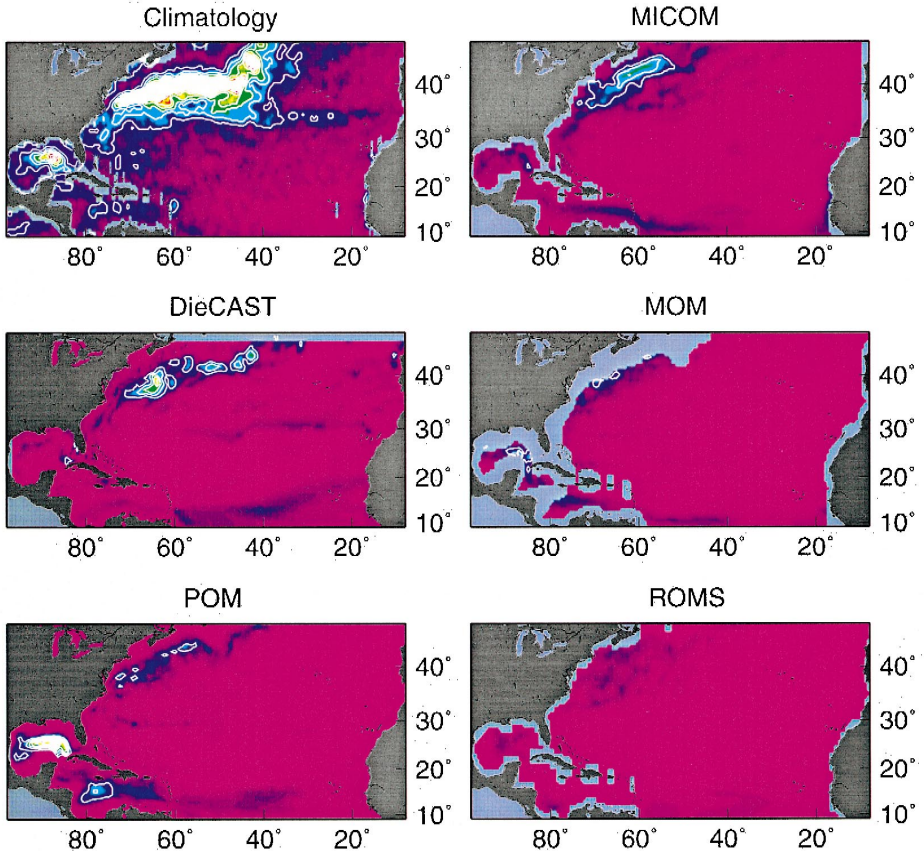


Fig. 6. Three-year sea surface height variability for the climatology (TOPEX 1992–1994) and for the five models. For MOM, the sea surface height was derived from the 1000 m geopotential height. The contour interval is 1×10^{-2} m.

variability is however present in the western South Atlantic (North Brazil current), in the Gulf of Mexico (Loop current), and in the Gulf Stream region. DieCAST exhibits the highest variability over the latter region, while, in the Gulf of Mexico, the highest eddy variability is exhibited by POM. The variable curvilinear grid of POM has the finest resolution (20–30 km) in that region, leading to a better representation of baroclinic instabilities. Because of its coarser grid ($3/4^\circ$), ROMS eddy activity is the weakest overall. Finally, the variability of the Loop Current and of the Gulf Stream in MOM is on time scales of roughly 6 months and 3–4 years, respectively (as indicated by a 20-year integration carried out by C.-C. Ma and C.R. Mechoso, and analyzed by A. Wirth, K. Ide, and M. Ghil; not shown).

Despite the fact that the SST fields are strongly constrained by the heat flux formulation (Eq. 1), the annual mean fields (Fig. 7) show differences that are characteristic of each model's surface circulation and that primarily result from the western boundary current representation. Consequently, there is no slope water signature in the

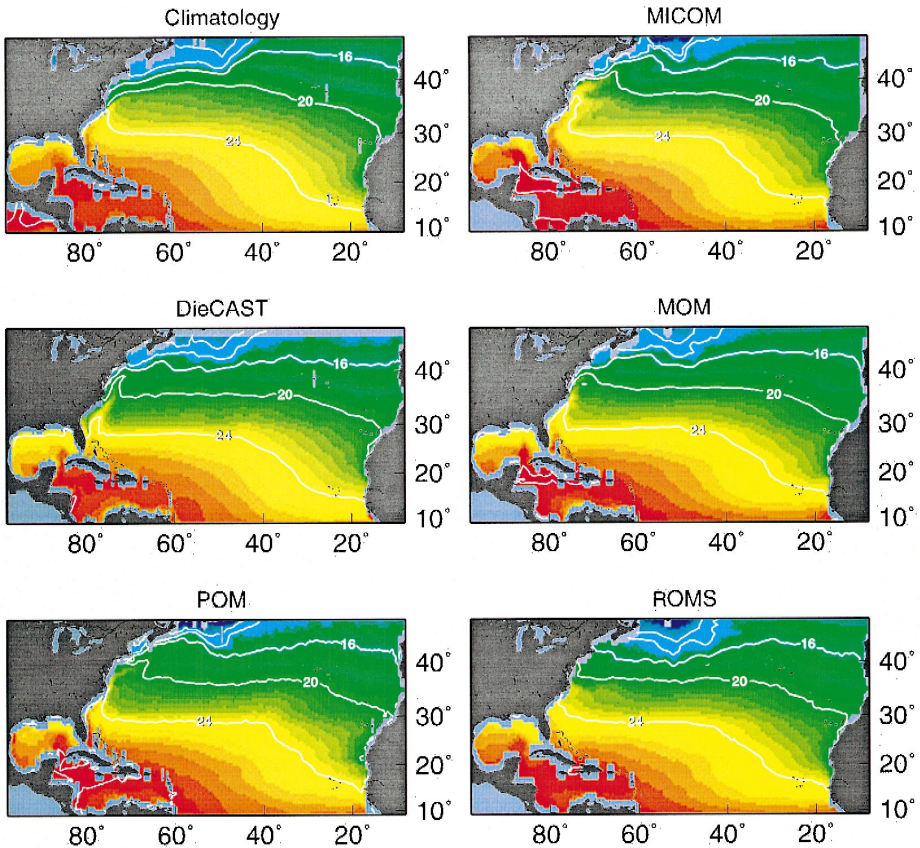


Fig. 7. Time average sea surface temperature for the climatology and five models over the last 3 years. The contour interval is 4°C .

models that exhibit an overshooting Gulf Stream at Cape Hatteras, which advects warm subtropical water too far north. ROMS, with its southern Gulf Stream separation, is the exception and some slope water is represented in that simulation. As for the SSH variability, the SST variability (Fig. 8) is mostly generated by the seasonal atmospheric forcing. All models fail to represent the high variability in the slope water. In addition, two models (MOM and POM) exhibit higher variability than observed in the middle of the subtropical gyre.

4.3. Barotropic transport at 27°N

Transport variations are observed in the western boundary current as a result of the seasonal forcing fluctuations, as shown by measurements in the Florida Straits (Schott et al., 1988; Larsen, 1992) and off the Bahamas Islands (Lee et al., 1990). Given that the models' grid spacing does not resolve the Florida Straits, a direct comparison of the

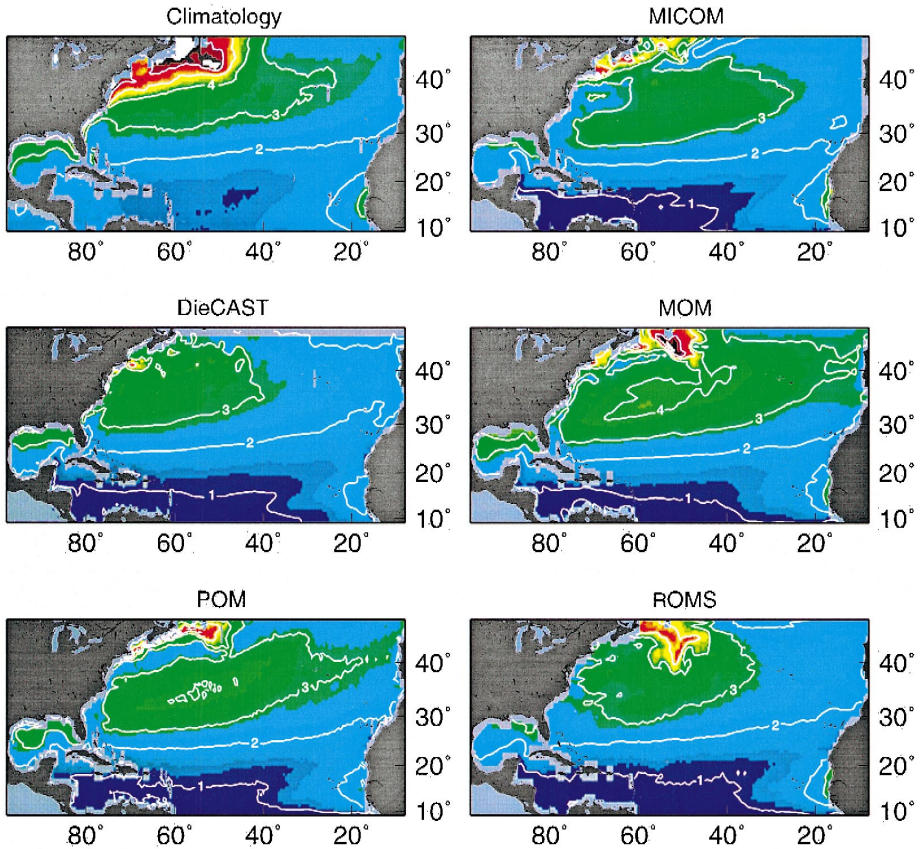


Fig. 8. Sea surface temperature variability for the climatology and the five models over the last 3 years. The contour interval is 1°C.

modeled Florida Straits transport to observations is meaningless. One can, however, for a given latitude, look at the vertically integrated transport as a function of longitude in order to quantify the seasonal variations in transport in the western boundary current and in the interior. The 27°N latitude was chosen since the transport at that latitude should obey the Sverdrup balance, at least in the eastern basin. The 3-year time-averaged vertically integrated transport as a function of longitude is therefore displayed in Fig. 9c, together with the corresponding Sverdrup transport (flat bottom).

ROMS and MICOM agree well with the Sverdrup balance east of 70°W . In MOM, however, there is a strong deviation from the Sverdrup balance west of 50°W with an interior transport in excess of 50 Sv, a result opposite to that obtained in DYNAMO (1997), in which the LEVEL model (similar to MOM) closely followed the Sverdrup

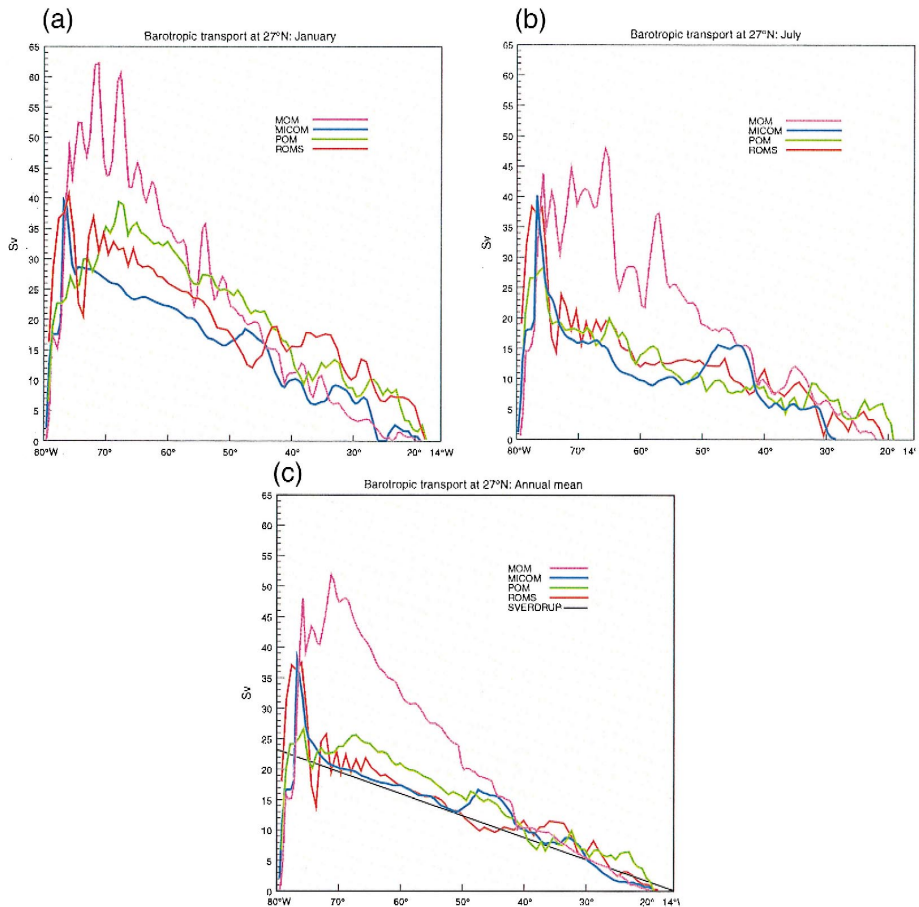


Fig. 9. Barotropic transport in Sverdrups at 27°N for MICOM, MOM, POM, and ROMS. (a) 3-year January mean, (b) 3-year July mean, (c) 3-year annual mean.

balance. ROMS, on the other hand, behaves more like the SIGMA coordinate model in DYNAMO (1997) by deviating from the Sverdrup balance east of 40°W. Willebrand et al. (2000) suggested that interactions of the baroclinic flow with bottom topography may be responsible for such deviations. If topography was the major factor responsible for the differences, then the signature of the Mid-Atlantic Ridge (the strongest topographic feature at 27°N) should also appear in the barotropic transport. Such a signature, however, is only visible in the MICOM simulation and the deviations observed in ROMS may therefore not be of topographic origin. These deviations are also not present in the other sigma coordinate simulation, POM. As stated by Willebrand et al. (2000), the correct model behavior cannot be evaluated at the present time for lack of conclusive direct observations.

The seasonal variations in the 27°N transport are illustrated in Fig. 9a,b for the months of January and July, respectively (3-year time average). The response to the seasonal forcing varies significantly among the models. MOM exhibits the most peculiar behavior with a maximum interior transport in excess of 60 Sv in January, clearly not in line with any observational estimates. Among the remaining three models, POM exhibits the largest variations in interior transport (~ 20 Sv at 65°W) when contrasted to MICOM and ROMS (~ 10 Sv at 65°W). POM also exhibits the largest seasonal transport in the western boundary current, with the maximum transport in July (Fig. 9b) located close to the western boundary. This maximum, however, migrates eastward by about 1000 km to 65°W in winter (Fig. 9a). The end result is that no signature of the western boundary current appears in the annual mean transport of POM at 27°N (Fig. 9c). By contrast, in both ROMS and MICOM, the western boundary current transport has a maximum close to the western boundary with small (5 Sv in ROMS) or zero (in MICOM) seasonal fluctuations. The signature of the deep western boundary current is also quite noticeable in these last two simulations.

4.4. Water mass properties

4.4.1. Ventilation of the interior

At mid-latitudes, the ventilation of the permanent thermocline results primarily from the subduction into the ocean interior of water masses formed through air–sea interaction near the ocean surface. Observations show that subduction, driven by the combined effects of Ekman pumping and geostrophic flow through the base of the late winter mixed layer (Marshall et al., 1993; Williams et al., 1995), occurs preferentially in certain density ranges, leading to the formation of relatively thick layers with homogenized properties, or mode waters (McCartney and Talley, 1982). In the North Atlantic, this process is characterized by the well-defined subtropical mode water (or 18°C water) that is formed in the Sargasso Sea and ventilates the interior at depths of 400–500 m.

The ventilation patterns can be characterized by the thicknesses of layers defined by a given potential density range, as illustrated by New et al. (1995) and Chassignet et al. (1996). Closed thickness contours represent the amount of fluid that has irreversibly left the mixed layer to enter the permanent pycnocline and resemble the subduction patterns of idealized thermocline models (Luyten et al., 1983; Williams et al., 1995). The

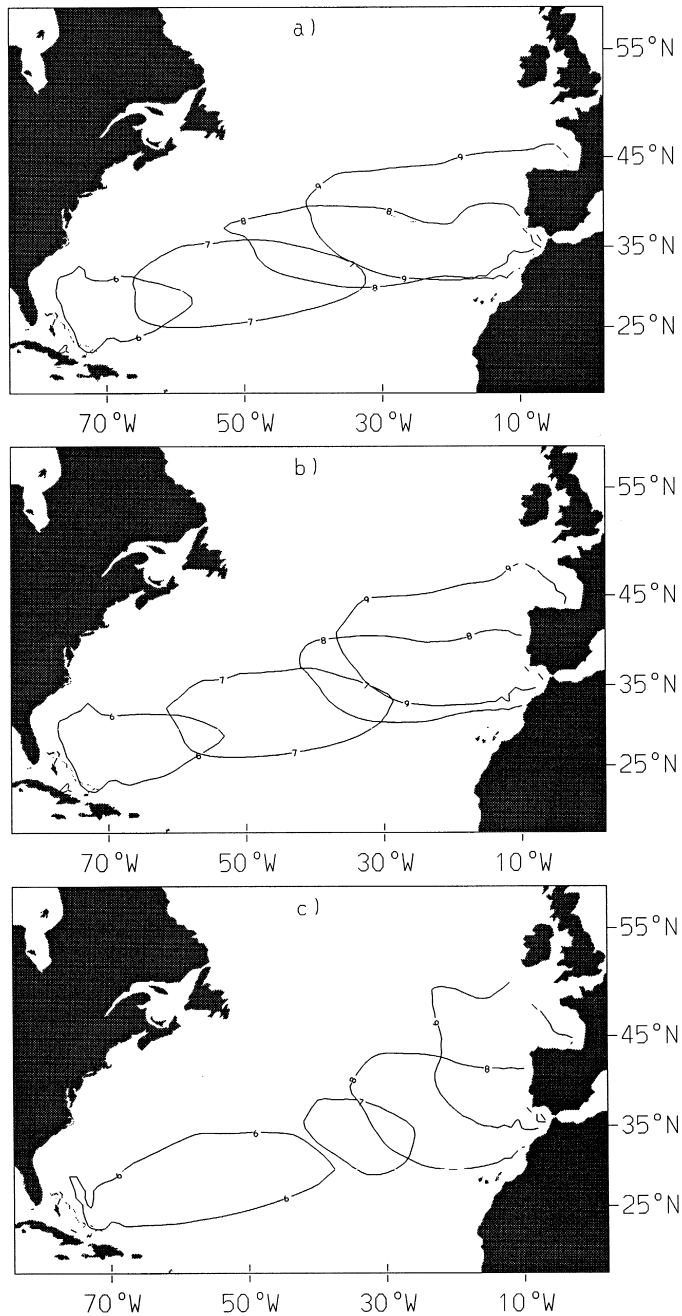


Fig. 10. Area (denoted by solid contours) in which a model layer thickness exceeds 200 m in the subtropical gyre, for layers 6 ($\sigma_\theta = 26.52$), 7 ($\sigma_\theta = 26.80$), 8 ($\sigma_\theta = 27.03$), and 9 ($\sigma_\theta = 27.22$), in March of year 20; (a) linearized heat flux, (b) bulk formula heat flux, and (c) same as (a), except for the relaxation to Levitus monthly surface salinity (instead of the prescribed $E - P$).

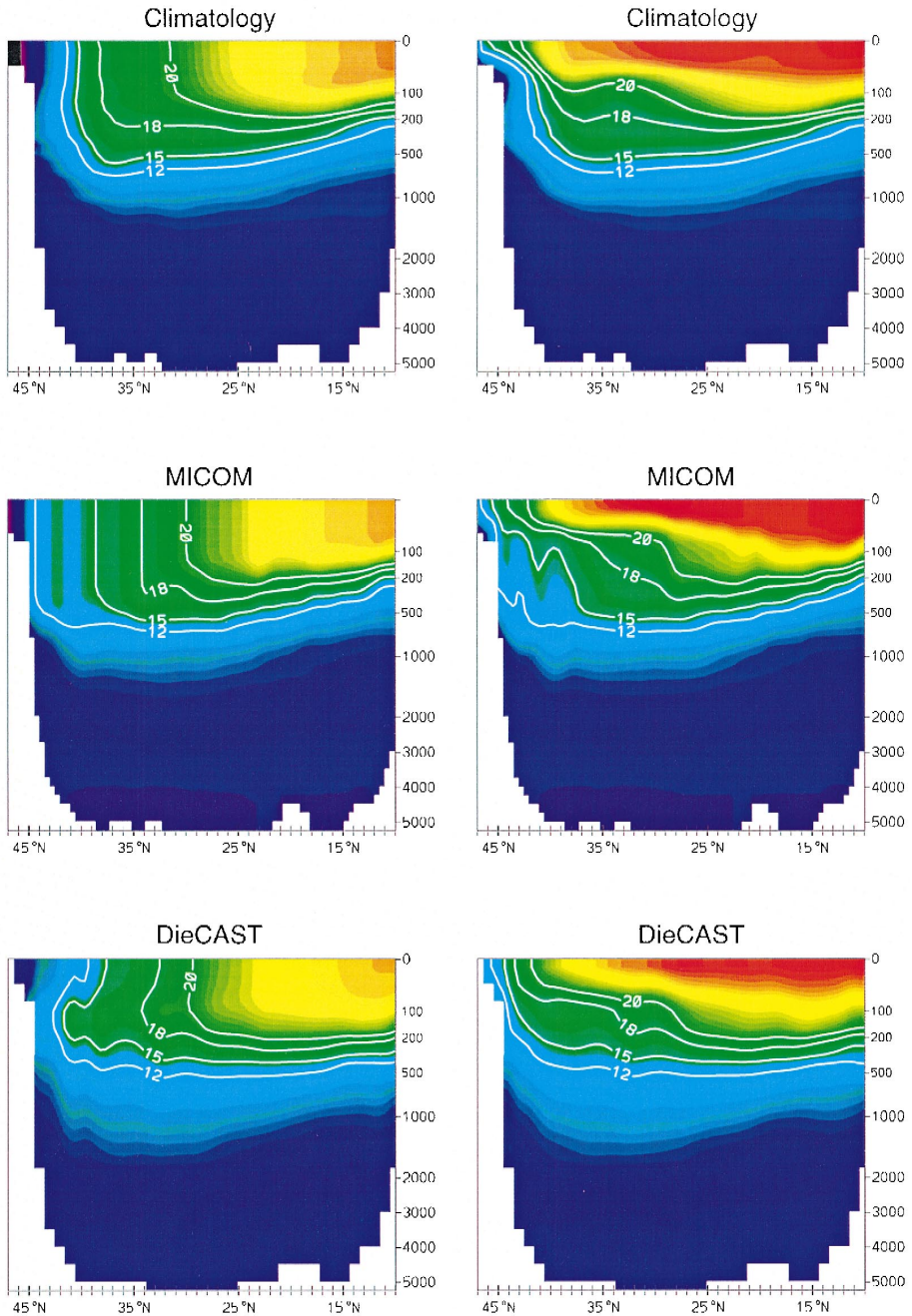


Fig. 11. Time average temperature cross-section at 55°W in February and August for the climatology, MICOM, and DieCAST. Time average temperature cross-section at 55°W in February and August for MOM, POM, and ROMS.

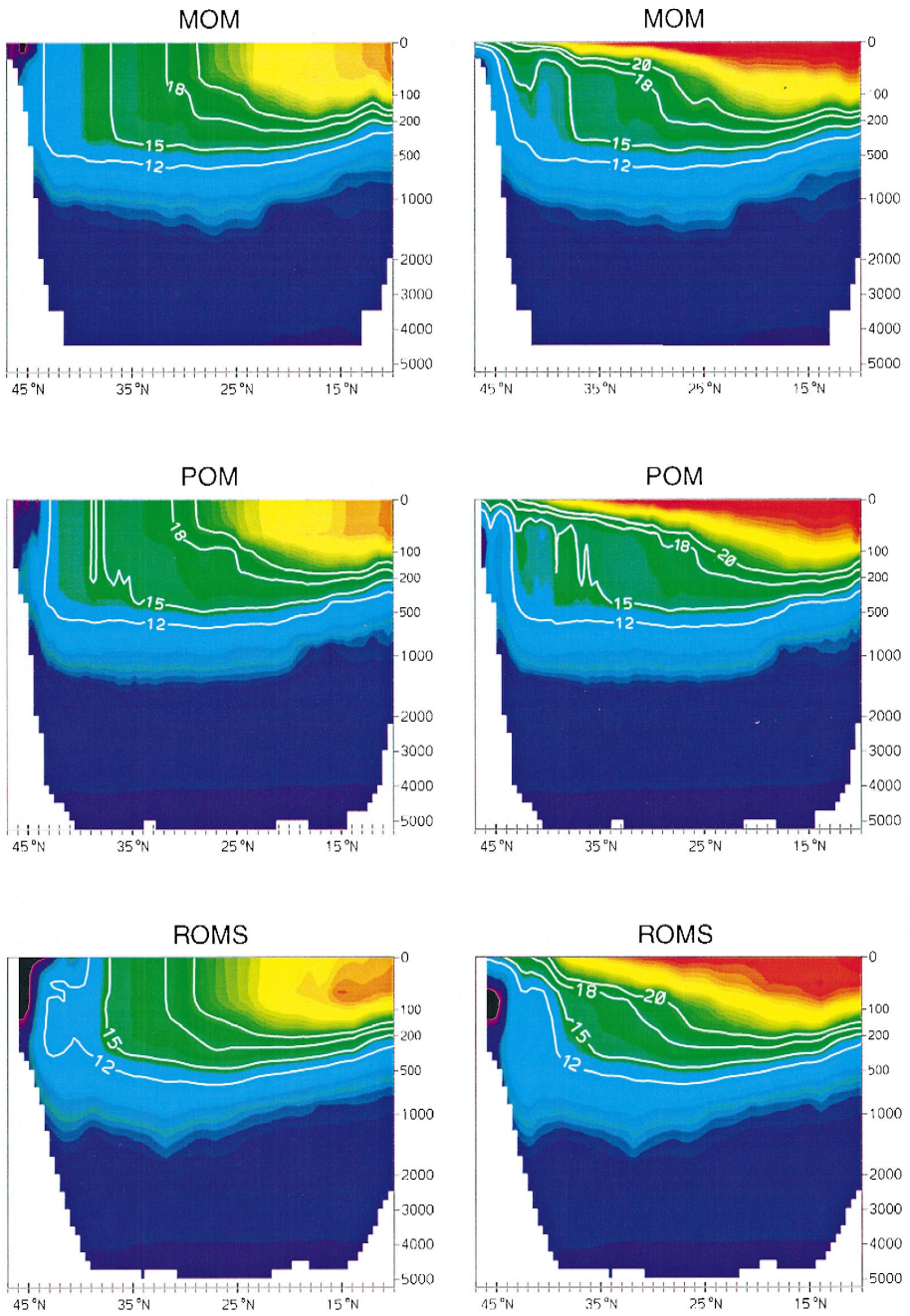


Fig. 11 (continued).

distribution of these patterns does depend on the model's architecture, as illustrated by Chassignet et al. (1996) in a model comparison between MOM and MICOM. Furthermore, this distribution also results from the choice of the surface forcing (heat and freshwater fluxes) since they directly affect the properties of the subducted fluid.

The importance of the choice of surface forcing is illustrated for several surface fluxes in a sensitivity study performed with MICOM. Fig. 10 shows the closed contours defining the region in which a particular layer thickness is greater than 200 m in March of the final year of each simulation. The lenses show a regular spatial progression, with lighter waters ventilating the western part of the domain and heavier waters ventilating the eastern part. The ventilation patterns for each layer are functions of the properties of the late-winter mixed layer, with an eastward (westward) shift of the ventilation source corresponding to a decrease (increase) in the wintertime mixed layer (New et al., 1995).

The ventilation patterns are very similar for a heat flux expressed either by the linearized bulk formula of Eq. 1 (Fig. 10a) or by the full bulk formula (Bleck et al., 1992) using COADS atmospheric data (Fig. 10b). The small northeastward displacement of the subduction lenses in the latter experiment, when contrasted to that of the former, reflects a warmer, and consequently lighter, subtropical gyre. The formulation of the freshwater flux has a much stronger impact on the ventilation patterns, as shown in Fig. 10c for a case in which the $E-P$ forcing was replaced by a surface relaxation to Levitus (1982) monthly surface salinity. In this case, the subtropical gyre is much fresher and lighter than shown in Fig. 10a, and the outcropping region is displaced eastward, with the denser layers ventilating primarily the eastern basin and the lighter layers occupying most of the Sargasso Sea. The sensitivity of the model's solution to the freshwater flux formulation was also investigated using ROMS by Haidvogel et al. (2000, this issue).

In order to illustrate the subduction process in the various models, Fig. 11 displays the meridional sections of temperature at 55°W in February and August (3-year mean). The surface forcing is that described in Section 2, i.e., a linear bulk formula for the heat flux and $E-P$ surface forcing. When compared to the climatological values, the winter mixed layer depth in all models is of comparable magnitude, except for that in DieCAST where the temperature is not as well mixed. DieCAST is also the only model that does not form any mode water. The characteristics of the formed mode water vary from one model to the other, with cooler temperatures than observed in MOM, POM, and ROMS, and temperatures closer to 18°C in MICOM. As discussed in the context of Fig. 10, this implies that either denser layers in MOM, POM, and ROMS are being ventilated in the western basin in comparison to MICOM, or that salinity underwent a significant modification within the ventilated layer. Finally, it is worth noting that the two models that use the Mellor–Yamada turbulence scheme, MOM and POM, exhibit summertime thermocline that is too shallow north of 30°N (Fig. 11). This is a common problem of models that use the Mellor–Yamada turbulence scheme. An improved version of this scheme (Mellor, 2000) as well as the addition of short wave radiation penetration greatly improved the mixed-layer behavior in POM for the same configuration (Ezer, 2000).

4.4.2. Maintenance of the Mediterranean salt tongue

Since one cannot appropriately model the Straits of Gibraltar with the chosen horizontal grid resolution, the outflow of Mediterranean waters into the North Atlantic

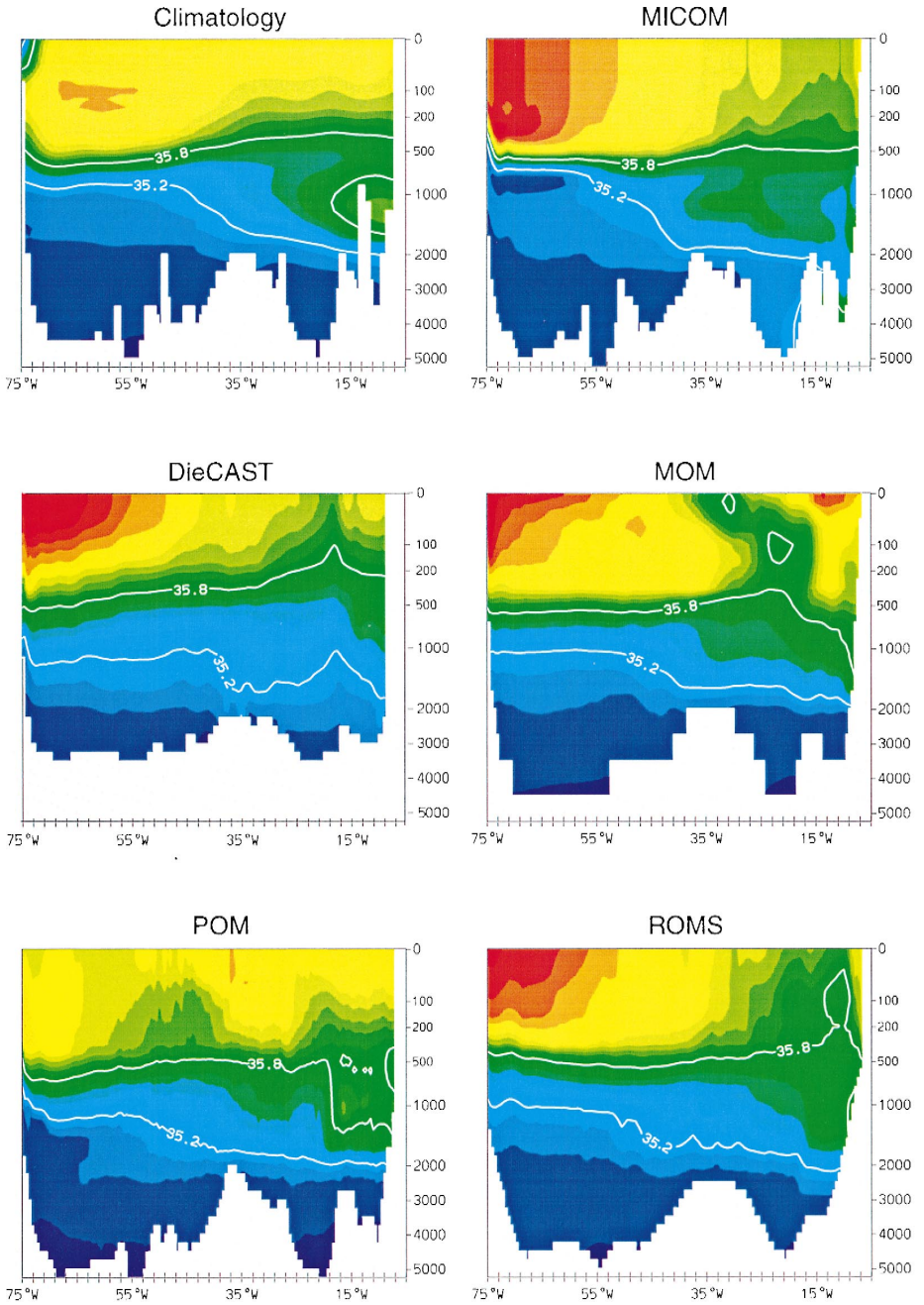


Fig. 12. Time average salinity cross-section at 35°N for the climatology and the five models over the last 3 years.

was simulated in most models by restoring the water mass properties to climatological values in a small buffer zone located in the Gulf of Cádiz. Observations show that waters with high salinity from the Mediterranean Sea flow into the Gulf of Cádiz, mix with the overlying waters, and then circulate and are subjected to further mixing in the North Atlantic. The signature of the Mediterranean outflow can be followed in observations across the subtropical gyre, up to the western basin, as a salinity maximum at depths around 1000 m (Arhan, 1987). A comprehensive view of the outflow and mixing of the Mediterranean waters has been given by Baringer and Price (1997). The source Mediterranean water, with $S \geq 38.4$ and $\sigma_\theta \geq 28.95$, flows through the Straits of Gibraltar into the Gulf of Cádiz as a bottom current. There, mixing with the fresher central water of the North Atlantic generates a neutrally buoyant water at depths near 1000 m, with $36.35 \leq S \leq 36.65$ and $27.3 \leq \sigma_\theta \leq 27.7$. This water then leaves the Gulf of Cádiz through its northern part and flows into the North Atlantic.

Salinity sections at 37°N are presented in Fig. 12 for the Levitus (1982) climatology and for all models (3-year average). The relaxation boundary condition is in general capable of reproducing some of the Mediterranean salinity water intrusion, although with lower salinity in most cases. The intrusion in POM is the most vigorous, but its structure has been partially eroded due to some homogenization with the overlying water. The upper salinities (less than 500 m) in POM are closer to the climatological values than in the other models. This is a direct consequence of the fact that relaxation to climatological salinity is performed in POM for the upper 5 sigma-levels (see Section 3.2.1 for more details). All other models exhibit a salinity drift as a consequence of the $E-P$ forcing (Paiva et al., 2000; Haidvogel et al., 2000, both in this issue), especially in the western boundary current. The intrusion's signature is the weakest in DieCAST while the signatures in ROMS and MOM resembles that in POM in the sense that mixing with the overlying water has also taken place. It is worthwhile recalling at this point that MOM is the only one of the five models that actually includes part of the Western Mediterranean in its domain.

MICOM exhibits a somewhat different behavior with a partially homogenized salinity structure near the eastern boundary, around values of 35.6 psu (lower than observed). Paiva et al. (2000, this issue) showed that this decrease in model salinity is not a continuous trend during the integration time (which would eventually cause the disappearance of the salinity intrusion), but rather is evidence that the model seeks an equilibrium state in which the mid-depth salinity intrusion is weaker than that in the observations. A removal of the buffer zone in the Gulf of Cádiz almost completely erases the salinity intrusion (Paiva et al., 2000, this issue).

5. Summary and discussion

The results of an intercomparison experiment performed with five numerical models of different architecture have been presented, with the objective of evaluating the capabilities of several of the models presently available to the oceanographic community. As in DYNAMO (Willebrand et al., 2000), all models are able to simulate the large-scale characteristics of the North Atlantic circulation with a fair degree of realism.

In some cases, the degree of realism was affected by the choice that was made for the domain's configuration. The domain size (6°N–50°N) is smaller than that used in other model comparisons (Chassignet et al., 1996; Willebrand et al., 2000) and places the domain boundaries across western boundary currents. When compared to large domain experiments, the results obtained with ROMS for the small domain were in general inferior (Haidvogel et al., 2000, this issue), with a lower meridional overturning streamfunction maximum and lower heat transport (by about 40%). Other models, however, such as MICOM (Paiva et al., 2000, this issue), found very little differences between results obtained in the large and small domains. This may be related to the way in which the various models implement the relaxation to climatological values in the buffer zones (Killworth, 1999). In isopycnic coordinate models such as MICOM, relaxation to salinity and layer interface depth is analogous to relaxation to salinity and temperature in level and sigma models only as long as the vertical density gradients in the model and in the observations are sufficiently close to one another.

The two level models, MOM and DieCAST, exhibit the traditional excessive up-welling around 35°N when integrated without a parameterization that minimizes the unphysical diapycnal mixing (Böning et al., 1995) due to numerical truncation errors (Veronis, 1975; Gent and McWilliams, 1990; Böning et al., 1995; Griffies et al., 1998, 2000). Level and sigma coordinate models rely on numerical convergence to model adiabatic advection, which is built into the algorithmic framework of isopycnic coordinate models. Griffies et al. (2000) shows the importance of adequately resolving the scale of motion in order to maintain a small amount of mixing consistent with that measured within the ocean. If not carefully tuned (horizontal and vertical grid, advection scheme), level and sigma coordinate models can manifest unphysically large amounts of diapycnal mixing due to numerical truncation errors (Griffies et al., 2000). Isopycnic coordinate models do not have this problem, but do suffer from the fact that they must use a single potential density to maintain the above-described adiabaticity. The difficulty was illustrated in Section 4.1, in which it was shown that MICOM was unable to simulate the water mass distribution associated with AABW. This deficiency can be remedied by adopting a 2000 dbar reference (instead of the surface) as well as a “virtual” density which almost eliminates the pressure gradient error associated with the use of a single potential density (Sun et al., 1999).

The surface fields were found to be similar in most experiments with the exception of ROMS, which exhibits, in both the small and large domains, a southern Gulf Stream path (at approximately the observed latitude). This result must be contrasted with the typical western boundary current overshoot that is present in most published coarse resolution experiments. The precursor of ROMS, i.e., SPEM, also exhibits a similar tendency for an early Gulf Stream detachment in coarse resolution experiments (Dengg et al., 1996; Knochel, 1998; Beckmann, 2000, personal communication). This early separation cannot, however, be characterized as a property of terrain-following coordinate models, since POM, another sigma coordinate model, does not show this behavior. With SPEM, this tendency disappears in experiments with higher resolution (1/3°) (DYNAMO, 1997; Willebrand et al., 2000).

A useful diagnostic, first introduced by the DYNAMO group, is a detailed comparison of the annual mean barotropic transport at a given latitude. In this paper, the

seasonality of this transport was also discussed. The differences among the models are quite large for reasons that are not yet clear. The level model MOM strongly deviates from the Sverdrup balance, a result opposite to that obtained in DYNAMO (1997), in which the LEVEL model (similar to MOM) closely followed the Sverdrup balance. The seasonal variations in the magnitude of the interior transport are largest in POM (when contrasted to ROMS and MICOM), with a maximum that migrates eastward by a thousand kilometers in winter. By contrast, in both ROMS and MICOM, the maximum is always associated with the western boundary current.

None of the models were able to maintain the Mediterranean salt tongue despite the imposed relaxation boundary condition in the Gulf of Cádiz (or the inclusion of part of the Western Mediterranean in MOM). Observations show that the salinity intrusion results from mixing of high salinity water from the Mediterranean Sea with overlying North Atlantic waters. This intense mixing takes place primarily via Kelvin–Helmholtz instabilities on scales on the order of tens of meters (Baringer and Price, 1997), a process clearly not resolved by present basin scale numerical simulations. There is therefore a strong need for a proper parameterization of this mixing process. The lack of a proper parameterization of the entrainment associated with overflows can lead to large differences in water mass composition, as illustrated by the DYNAMO results in the Denmark Straits and the Greenland–Scotland overflows (Willebrand et al., 2000).

Clearly, none of the models performs equally well in every aspect of the North Atlantic circulation. Ideally, an Ocean General Circulation Model (OGCM) should (a) retain its water mass characteristics for centuries (a characteristic of isopycnic coordinates), (b) have high vertical resolution in the surface mixed layer (a characteristic of z -level coordinates) for proper representation of thermodynamical and biochemical processes, (c) maintain sufficient vertical resolution in unstratified or weakly-stratified regions of the ocean, and (d) have high vertical resolution in coastal regions (a characteristic of terrain-following coordinates). Comparison exercises like DYNAMO and DAMÉE illustrate the strengths and weaknesses of each approach (characterized mostly by the choice in vertical coordinates). The results of these exercises have led to the recent development of several hybrid coordinate numerical models that combine the advantages of the different types of coordinates in optimally simulating coastal and open-ocean circulation features.

Acknowledgements

This work was part of DAMÉE-NAB which was supported by the Office of Naval Research Ocean Modeling and Prediction Program (M. Fiadeiro and T. Curtin). This support is gratefully acknowledged. We would like to also thank A. Beckmann, K. Hedström, P. Hogan, H. Hurlburt, K. Ide, A. Mariano, C.R. Mechoso, G. Mellor, W. Schmitz, R. Willems, and A. Wirth for their participation in DAMÉE-NAB. Most of the computations were carried out on the computers of the Department of Defense (DoD) at the Stennis Space Center. Additional computational resources were provided by NOAA/GFDL.

References

- Arhan, M., 1987. On the large scale dynamics of the Mediterranean outflow. *Deep Sea Res.* 34, 1187–1208.
- Baringer, M.O., Price, J.F., 1997. Mixing and spreading of the Mediterranean outflow. *J. Phys. Oceanogr.* 27, 1654–1676.
- Bleck, R., Rooth, C.G.H., Hu, D., Smith, L.T., 1992. Salinity-driven thermocline transients in a wind- and thermohaline-forced isopycnic coordinate model of the North Atlantic. *J. Phys. Oceanogr.* 22, 1486–1505.
- Bleck, R., Chassignet, E.P., 1994. Simulating the oceanic circulation with isopycnic-coordinate models. In: Majumdar, S.K., Miller, E.W., Forbes, G.S., Schmalz, R.F., Panah, A.A. (Eds.), *The Oceans: Physical–Chemical Dynamics and Human Impact*. The Pennsylvania Academy of Science, pp. 17–39.
- Blumberg, A.F., Mellor, G.L., 1987. A description of a three-dimensional coastal ocean circulation model. In: Heaps, N.S. (Ed.), *Three-Dimensional Coastal Ocean Models* vol. 4 American Geophysical Union, Washington, DC, pp. 1–16.
- Böning, C.W., Herrmann, P., 1994. Annual poleward heat transport in the ocean. Results from high-resolution modeling of the North and Equatorial Atlantic. *J. Phys. Oceanogr.* 24, 91–105.
- Böning, C.W., Holland, W.R., Bryan, F.O., Danabasoglu, G., McWilliams, J.C., 1995. An overlooked problem in model simulations of the thermohaline circulation and heat transport in the Atlantic Ocean. *J. Clim.* 8, 515–523.
- Browning, G.L., Henshaw, W.D., Kreiss, H.-O., 1998. A numerical investigation of the interaction between the large and small scales of the two-dimensional incompressible Navier–Stokes equations. *CAM Report* 98-23, April 1998, UCLA.
- Bryan, K., 1969. A numerical method for the study of the circulation of the world ocean. *J. Comput. Phys.* 4, 347–376.
- Chassignet, E.P., Bleck, R., Rooth, C.G.H., 1995. The influence of layer outcropping on the separation of boundary currents: Part II. The wind- and buoyancy-driven experiments. *J. Phys. Oceanogr.* 25, 2404–2422.
- Chassignet, E.P., Smith, L.T., Bleck, R., Bryan, F.O., 1996. A model comparison: Numerical simulations of the North and Equatorial Atlantic oceanic circulation in depth and isopycnic coordinates. *J. Phys. Oceanogr.* 26, 1849–1867.
- Cox, M.D., 1984. A primitive equation, 3-dimensional model of the ocean. GFDL Ocean Group Tech. Rep. No. 1, Geophysical Fluid Dynamics Laboratory/NOAA Princeton University, Princeton, New Jersey.
- da Silva, A.M., Young, C.C., Levitus, S., 1994. Atlas of surface marine data 1994, Volume 3, Anomalies of heat and momentum fluxes. NOAA Atlas NESDIS 8, 413 pp., NOAA, Washington, DC.
- Dengg, J., Beckmann, A., Gerdes, R., 1996. The Gulf Stream separation problem. In: Krauss, W. (Ed.), *The warmwatersphere of the North Atlantic Ocean*. Gebr. Borntraeger, Berlin, pp. 253–290.
- Dietrich, D.E., 1997. Application of a modified A-grid ocean model having reduced numerical dispersion to the Gulf of Mexico circulation. *Dyn. Atmos. Oceans* 27, 201–317.
- Dietrich, D.E., Ko, D.-S., 1994. A semi-collocated ocean model based on the SOMS approach. *Int. J. Numer. Methods Fluids* 19, 1103–1113.
- Dietrich, D.E., Lin, C.A., 1994. Numerical studies of eddy shedding in the Gulf of Mexico. *J. Geophys. Res.* 99, 7599–7615.
- Dietrich, D.E., Lin, C.A., Mestas-Nunez, A., Ko, D.-S., 1997. A high resolution numerical study of Gulf of Mexico fronts and eddies. *Met. Atm. Phys.* 64, 187–201.
- Dietrich, D.E., Mehra, A., 1998. Explosive convective adjustment in a hydrostatic ocean model. MSU-CAST, Technical Report 02-98.
- DYNAMO, 1997. Dynamics of North Atlantic Models. Simulation and assimilation with high resolution models. Institut für Meereskunde an der Universität Kiel, 334 pp.
- Ezer, T., 2000. On the seasonal mixed-layer simulated by a basin-scale ocean model and the Mellor–Yamada turbulence scheme. *J. Geophys. Res.*, submitted for publication.
- Ezer, T., Mellor, G.L., 1992. A numerical study of the variability and the separation of the Gulf Stream induced by surface atmospheric forcing and lateral boundary flows. *J. Phys. Oceanogr.* 22, 660–682.
- Ezer, T., Mellor, G.L., 2000. Sensitivity studies with the North Atlantic Princeton Ocean model. *Dyn. Atmos. Oceans* 32, 185–208.
- Gent, P.R., McWilliams, J.C., 1990. Isopycnal mixing in ocean circulation models. *J. Phys. Oceanogr.* 20, 150–155.

- Griffies, S.M., Gnanadesikan, A., Pacanowski, R.C., Larichev, V., Dukowicz, J.K., Smith, R.D., 1998. Isoneutral diffusion in a z -coordinate ocean model. *J. Phys. Oceanogr.* 28, 805–830.
- Griffies, S.M., Pacanowski, R.C., Hallberg, R.W., 2000. Spurious diapycnal mixing associated with advection in a z -coordinate ocean model. *Mon. Weather Rev.*, in press.
- Haidvogel, D.B., Wilkin, J.L., Young, R.E., 1991. A semi-spectral primitive equation ocean model using vertical sigma and orthogonal curvilinear horizontal coordinates. *J. Comput. Phys.* 94, 151–185.
- Haidvogel, D.B., Beckmann, A., 1999. In: *Numerical Ocean Circulation Modeling*. Imperial College Press, London, 318 pp.
- Haidvogel, D.B., Arango, H.G., Hedström, K.S., Beckmann, A., Malanotte-Rizzoli, P., Shchepetkin, A.F., 2000. Model evaluation experiments in the North Atlantic basin: simulations in nonlinear terrain-following coordinates. *Dyn. Atmos. Oceans* 32, 239–281.
- Jiang, S., Jin, F.-F., Ghil, M., 1995. Multiple equilibria, periodic and aperiodic solutions in a wind-driven, double-gyre, shallow-water model. *J. Phys. Oceanogr.* 25, 764–786.
- Killworth, P.D., 1999. Relaxation towards observations in level and isopycnal models. *J. Atmos. Ocean Tech.* 16, 983–986.
- Klinck, J.M., 1995. Thermohaline structure of an eddy-resolving North Atlantic model. The influence of boundary conditions. *J. Phys. Oceanogr.* 25, 1174–1195.
- Knochel, H., 1998. Développement et validation d'un modèle de circulation océanique à coordonnées σ pour l'étude climatique de l'Atlantique Nord. Thèse de l'Université Joseph Fourier, Grenoble.
- Kreiss, H.-O., Ystrom, J., 1998. A numerical study of the solution to the 3D incompressible Navier–Stokes equations. CAM Report 98-24, April 1998, UCLA.
- Large, W.G., McWilliams, J.C., Doney, S.C., 1994. A Review and model with a nonlocal boundary layer parameterization. *Rev. Geophys.* 32, 363–403.
- Larsen, J.C., 1992. Transport and heat flux of the Florida Current at 27N derived from cross-stream voltages and profiling data: theory and observations. *Philos. Trans. R. Soc. London* 338, 169–236.
- Lee, H., 1997. A Gulf Stream Synthetic Geoid for the TOPEX Altimeter. M.S. Thesis, Rutgers University, New Brunswick, New Jersey, 36 pp.
- Lee, T.N., Johns, W., Schott, F., Zantopp, R., 1990. Western boundary current structure and variability east of Abaco, Bahamas at 26.5°N. *J. Phys. Oceanogr.* 20, 446–466.
- Levitus, S., 1982. Climatological Atlas of the World Ocean. Professional Paper 13, NOAA, 173 pp.
- Luyten, J.R., Pedlosky, J., Stommel, H., 1983. The ventilated thermocline. *J. Phys. Oceanogr.* 13, 292–309.
- Macdonald, A.M., Wunsch, C., 1996. An estimate of global ocean circulation and heat fluxes. *Nature* 382, 436–439.
- Marshall, J.C., Nurser, A.J.G., Williams, R.G., 1993. Inferring the subduction rate and period over the North Atlantic. *J. Phys. Oceanogr.* 23, 1315–1329.
- McCartney, M.S., Talley, L.D., 1982. The subpolar mode water of the North Atlantic. *J. Phys. Oceanogr.* 12, 1169–1188.
- Mellor, G.L., 1991. An equation of state for numerical models of oceans and estuaries. *J. Atmos. Ocean Tech.* 8, 609–611.
- Mellor, G.L., 2000. One-dimensional, ocean surface layer modeling, a problem and a solution. *J. Phys. Oceanogr.*, submitted for publication.
- Mellor, G.L., Yamada, T., 1982. Development of a turbulence closure model for geophysical fluid problems. *Rev. Geophys. Space Phys.* 20, 851–875.
- Mellor, G.L., Ezer, T., Oey, L.-Y., 1994. The pressure gradient conundrum of sigma coordinate ocean models. *J. Atmos. Ocean Tech.* 11, 1126–1134.
- New, A.L., Bleck, R., Jia, Y., Marsh, R., Huddleston, M., Barnard, S., 1995. An isopycnal model study of the North Atlantic: Part I. Model experiment. *J. Phys. Oceanogr.* 25, 2667–2699.
- Özgökmen, T., Chassignet, E.P., Paiva, A., 1997. Impact of wind forcing, bottom topography and inertia on mid-latitude jet separation in a quasi-geostrophic model. *J. Phys. Oceanogr.* 27, 2460–2476.
- Paiva, A.M., Chassignet, E.P., Mariano, A.J., 2000. Numerical simulations of the North Atlantic subtropical gyre: sensitivity to boundary conditions and horizontal resolution. *Dyn. Atmos. Oceans* 32, 209–237.
- Phillips, N.A., 1957. A coordinate system having some special advantages for numerical forecasting. *J. Met.* 14, 184–185.

- Sanderson, B.G., 1998. Order and resolution for computational ocean dynamics. *J. Phys. Oceanogr.* 28, 1271–1286.
- Sanderson, B.G., Brassington, G., 1998. Accuracy in the context of a control–volume model. *Atmos.-Ocean* 36, 355–384.
- Schott, F.A., Lee, T.N., Zantopp, R., 1988. Variability of structure and transport of the Florida Current in the period range of days to seasonal. *J. Phys. Oceanogr.* 18, 1209–1230.
- Shchepetkin, A.F., McWilliams, J.C., 1998. Quasi-monotone advection schemes based on explicit locally adaptive dissipation. *Mon. Weather Rev.* 126, 1541–1580.
- Smagorinsky, J.S., 1963. General circulation experiments with the primitive equations: I. The basic experiment. *Mon. Weather Rev.* 91, 99–164.
- Smagorinsky, J., Manabe, S., Holloway, J.L., 1965. Numerical results from a nine-level general circulation model of the atmosphere. *Mon. Weather Rev.* 93, 727–768.
- Song, Y., Haidvogel, D.B., 1994. A semi-implicit ocean circulation model using a generalized topography-following coordinate. *J. Comput. Phys.* 115, 228–244.
- Sun, S., Bleck, R., Rooth, C.G.H., Dukowicz, J., Chassignet, E.P., Killworth, P., 1999. Inclusion of thermobaricity in isopycnic-coordinate ocean models. *J. Phys. Oceanogr.* 29, 2719–2729.
- Teague, W.J., Carron, M.J., Hogan, P.J., 1990. A comparison between the generalized digital environmental model and levitus climatologies. *J. Geophys. Res.* 95, 7167–7183.
- Veronis, G., 1975. The role of models in tracer studies. In: *Numerical Models of Ocean Circulations*. National Academy of Science, pp. 133–146.
- Willebrand, J., Barnier, B., Böning, C., Dietrich, C., Herrman, P., Killworth, P.D., LeProvost, C., Jia, Y., Molines, J.-M., New, A.L., 2000. Circulation characteristics in three eddy-permitting models of the North Atlantic. *Prog. Oceanogr.*, in press.
- Willems, R.C., Glenn, S.M., Crowley, M.F., Malanotte-Rizzoli, P., Young, R.E., Ezer, T., Mellor, G.L., Arango, H.G., Robinson, A.R., Lai, C.-C., 1994. Experiment evaluates ocean models and data assimilation in the Gulf Stream. *EOS, Trans., Am. Geophys. Union* 75 (34), 385–394.
- Williams, R.G., Spall, M.A., Marshall, J.C., 1995. Does Stommel’s mixed layer “demon” work? *J. Phys. Oceanogr.* 25, 3089–3102.